Influence of homogenisation treatments on the hot ductility of cast ATI® 718Plus®: Effect of niobium and minor elements on liquation characteristics

Materials Science & Engineering A 799 (2021) 140151

Contents lists available at ScienceDirect

Materials Science & Engineering A

journal homepage: http://www.elsevier.com/locate/msea

Influence of homogenisation treatments on the hot ductility of cast ATI® 718Plus®: Effect of niobium and minor elements on liquation characteristics

Sukhdeep Singh [a,*], Fabian Hanning [b], Joel Andersson [b]

[a] Department of Industrial and Materials Science, Chalmers University of Technology, Gothenburg, SE-41296, Sweden
[b] Department of Engineering Science, University West, Trollhättan, SE-46181, Sweden

ARTICLE INFO

Keywords:
HAZ Cracking
Niobium
Boron
Segregation
Diffusion
Constitutional liquation of carbides

ABSTRACT

The hot ductility of cast ATI® 718Plus® was assessed using the Gleeble thermo-mechanical simulator after being subjected to different homogenisation heat treatments. The hot ductility deteriorated significantly after long-dwell homogenisation heat treatments for 24 h at temperatures of 1120 and 1190 °C as compared with those treated at a short dwell time of 4 h at the same temperatures. The observed ductility deterioration was related to more extensive liquation along the grain boundaries caused by different mechanisms, e.g., liquation by solute segregation mechanism, Laves melting, constitutional liquation of MC carbides and supersolidus grain boundary melting, with the effect and extent depending on the solute changes after the homogenisation heat treatments. Furthermore, the role of Nb as the solute element and as the precipitate former, as well as the effect of minor alloying elements segregating along the grain boundaries, is discussed in connection to grain boundary liquation, which contributes to a better understanding of heat-affected zone liquation cracking susceptibility of cast ATI® 718Plus®.

1. Introduction

The Ni-base superalloy ATI® 718Plus® (718Plus) was developed in response to a demand by the aerospace industry for a material that could surpass the maximum operating temperature of Alloy 718 for improved engine performance. The newly developed 718Plus superalloy can be used at ~50 °C above the maximum temperature of 650 °C for Alloy 718 [1,2]. The better performance, while still maintaining good fabricability, led to the development project of the cast version of 718Plus for structural components under the Metals Affordability Initiative (MAI) programme led by major aerospace companies and suppliers [3]. Welding of Nb-bearing superalloys containing Laves phases, such as cast 718Plus and Alloy 718, can be challenging because of the significant segregation that remains in interdendritic areas from the solidification process, which can cause heat-affected zone (HAZ) liquation cracking during welding. Besides the Nb-rich Laves phase, minor elements such as P and B have been reported to increase the cracking susceptibility of 718Plus [4,5]. These elements have been attributed to lowering the liquation temperature and extending the solidification temperature range.

Prior to welding, cast components are subjected to homogenisation heat treatments or hot isostatic pressing (HIP) treatments to dissolve the detrimental Laves phase and to level out the elemental distribution. In a previous study by the authors [6], the effect of a set of homogenisation heat treatments in regard to their influence on weld HAZ cracking was investigated in cast 718Plus. It was found that the HAZ liquation cracking susceptibility of cast 718Plus was influenced by the homogenisation treatment dwell time rather than the soak temperature after Varestraint testing. Homogenisation heat treatments at 1120 and 1190 °C for 24 h exhibited higher cracking susceptibility than their counterparts treated for a dwell time of 4 h. Heat treatments that experienced enhanced homogenisation of the microstructure were more crack susceptible. Similarly, in another investigation on the repair welding behaviour of cast 718Plus, a reduced weld cracking susceptibility was seen for the Laves phase containing microstructures compared with material in which the Laves phase was completely dissolved [7]. The homogenisation heat treatments applied to 718Plus were based on the two different HIP treatment approaches developed for Alloy 718, which consists of the partial dissolution of the Laves phase at 1120 °C [8] and its total dissolution at 1190 °C [9,10]. A similar study was also

* Corresponding author.
E-mail addresses: sukhdeep.singh@chalmers.se (S. Singh), fabian.hanning@hv.se (F. Hanning), joel.andersson@hv.se (J. Andersson).

https://doi.org/10.1016/j.msea.2020.140151
Received 4 June 2020; Received in revised form 21 August 2020; Accepted 23 August 2020
Available online 27 August 2020

Table 1
Composition of cast 718 Plus in wt %.

Ni	Cr	Fe	Co	Nb	Mo	Al	Ti	W	Mn	Cu	Si	P	S	C	B
Bal.	20.72	9.31	8.34	6.02	2.71	1.5	0.75	1.00	0.01	<0.01	0.04	0.01	0.002	0.05	0.005

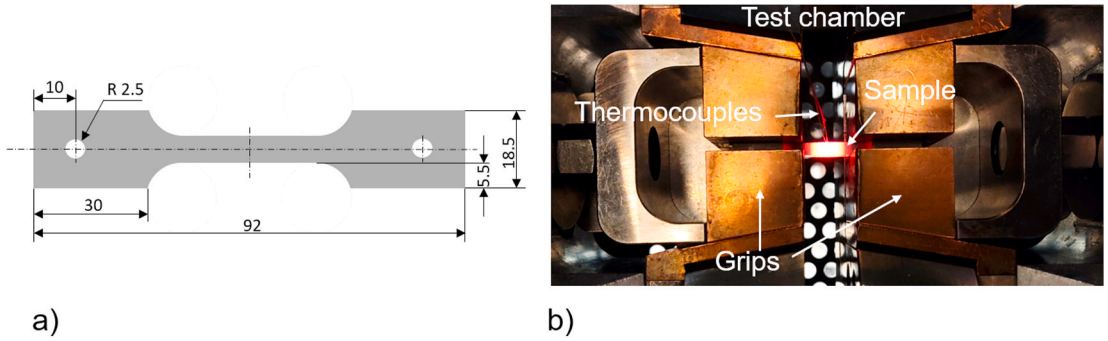

Fig. 1. (a) Gleeble test setup with sample heating, copper grips and thermocouple locations indicated by arrows. (b) Sample geometry and dimensions.

Table 2
Test parameters used for Gleeble testing.

Heating rate	Cooling rate	Peak temp.	Holding time	Free-span
111 °C/s	50 °C/s	1220 °C	0.03 s	20 mm

conducted on the weldability of cast Haynes® 282® [11]. The aim is to develop a unified heat treatment approach that minimises weld HAZ liquation cracking susceptibility in the three superalloys.

Hence, the scope of this study was to assess the hot ductility behaviour of cast 718Plus after homogenisation heat treatments with soak temperatures of 1120 and 1190 °C and dwell times of 4 and 24 h. The heat treatments were performed in a laboratory setup at ambient pressure. The effect of Nb and minor elements on the liquation characteristics was investigated and correlated to the HAZ liquation cracking susceptibility.

2. Experimental

Investment cast plates with approximate dimensions of 300 × 60 × 12 mm^3 and the chemical composition (in wt %) seen in Table 1 were received from the supplier.

Homogenisation heat treatments were performed at temperatures of 1120 and 1190 °C for dwell times of 4 and 24 h in a lab furnace, followed by water quenching. After homogenisation, the plates were cut by abrasive water jet cutting to the dimensions in Fig. 1 a. The hot ductility response was investigated by a Gleeble 3800D thermomechanical simulator. The test setup and parameters are, respectively, in Fig. 1 b and Table 2.

Tests were performed with a heating rate of 111 °C/s to various test temperatures with a holding time of 0.03 s, followed by a tensile load at a stroke rate of 55 mm/s until the samples fractured. During on-cooling tests, the specimens were heated to a peak temperature of 1220 °C and cooled at a rate of 50 °C/s. Two repetitions were made at each temperature. Subsequently, the area reduction at fracture surfaces was measured under a stereomicroscope. The hot ductility test also involved the measurement of different associated properties of the alloy, such as nil ductility temperature (NDT), nil strength temperature (NST), ductility recovery temperature (DRT) and brittle temperature range (BTR). The temperature at which the material possessed no ductility on-heating is referred to as NDT. The NST was measured by subjecting a sample to a load of about 100 N and heating until failure occurred. Hence, the failure temperature, where the sample did not sustain any strength, is termed NST. The DRT was measured during on-cooling tests. The temperature at which the material exhibited 5% ductility is referred to as DRT. BTR was determined by the difference between peak temperature (1220 °C) and DRT.

Cross-sections from the thermally simulated area were cut, mounted, grinded and finally polished with 9 and 3 μm discs with a diamond solution. Etching was conducted using oxalic acid at 3.2 V on polished samples for microstructure evaluation by light optical microscope and scanning electron microscope (SEM). For the latter, back-scattered (BS) and secondary electron (SE) modes were used in an LEO 1550 FEG-SEM, which was also equipped with Oxford energy dispersive X-ray spectroscopy (EDS). ToF-SIMS (time of flight secondary ion mass spectroscopy) analysis was performed to detect minor elements using a TOF. SIMS 5 instrument (ION-TOF GmbH, Münster, Germany) using a 25 kV Bi cluster ion gun as the primary ion source and a 10 kV Cs ion source for sputtering. The samples were analysed using a pulsed primary ion beam (Bi_3^+ at 0.2 pA) in the delayed extraction mode with a focus of approximately 400 nm. All spectra were acquired and processed with the Surface Lab software (version 6.4, ION-TOF GmbH, Münster, Germany). The spectra were internally calibrated to signals of $[C]^+$, $[CH_2]^+$, $[CH_3]^+$ and $[Cr]^+$ for the positive ion mode and $[C]^-$, $[CH]^-$, $[C_2]^-$ and $[Si]^-$ for the negative ion mode. Samples were etched using the Cs^+ beam at 20 nA/3kV. JMatPro v11 was used to model homogenisation and solidification behaviour.

3. Results

3.1. Base metal microstructure

The as-cast condition was characterised by highly segregated interdendritic areas in which the Laves phase and MC carbides were present, as shown in Fig. 2. Homogenisation heat treatments were able to dissolve the Laves phase, except for the one at 1120 °C/4 h, which exhibited partial Laves dissolution. From the previous study [7], the area fraction of secondary precipitates varied from about 5.2 wt % in the as-cast condition to about 2.6 wt % at 1120 °C/4 h down to about 0.5 wt % in all other heat treated conditions, which was attributed to the area fraction of MC carbides in the material. In the material heat-treated at 1190 °C/4 h, some MC carbides were surrounded by eutectic structures, suggesting that remelting had occurred, as shown in Fig. 2 d.

Base metal hardness decreased from the initial value of about 410 HV to 330–350 HV after the homogenisation heat treatments, whereas grain size was stable at an average value of about 1.3 mm [7]. SIMS analysis revealed the segregation of different elements along the grain

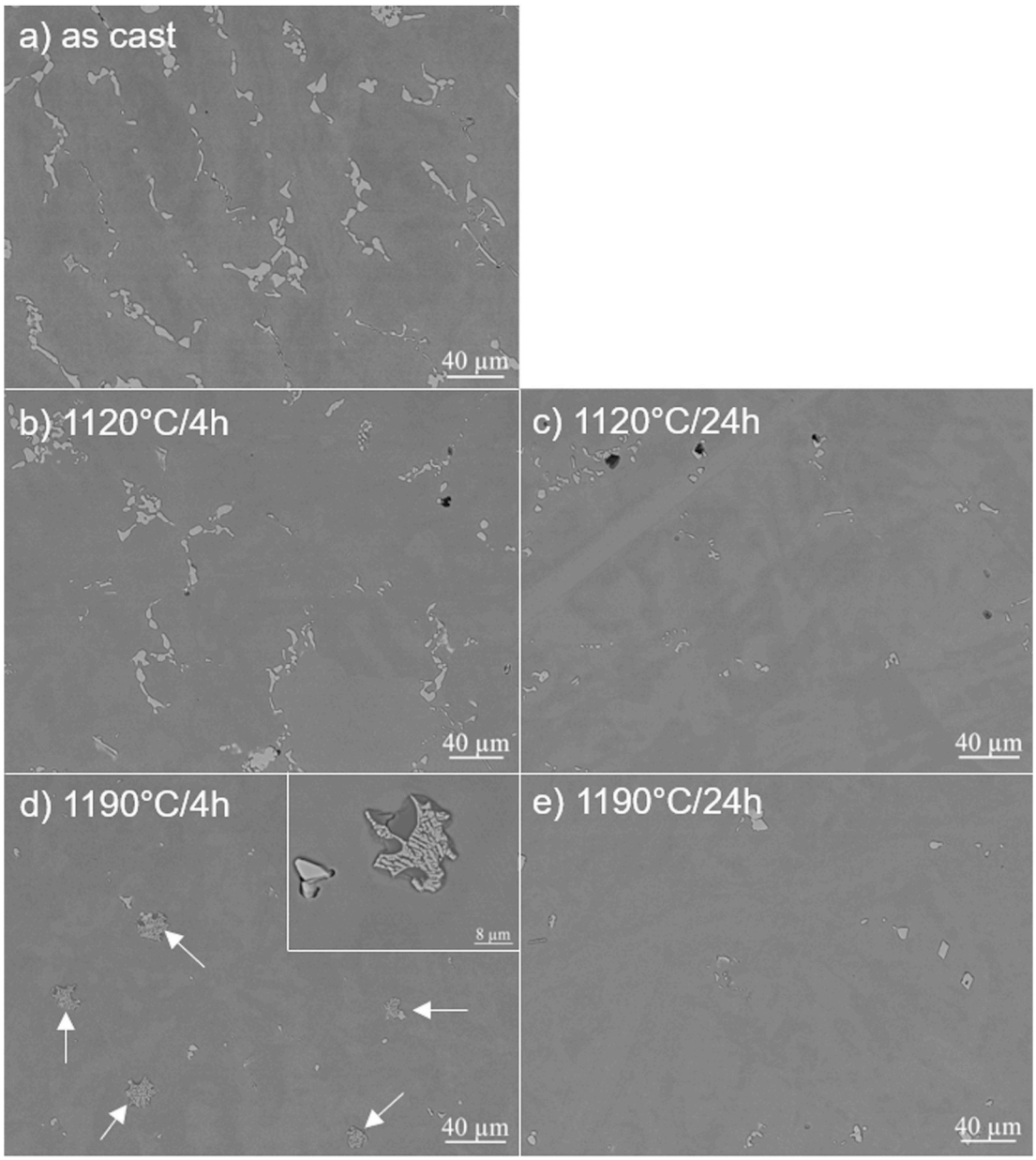

Fig. 2. Base metal microstructure in (a) as-cast and after homogenisation heat treatments at (b) 1120 °C/4 h, (c) 1120 °C/24 h, (d) 1190 °C/4 h, with the small insert shows remelting of a carbide, and (e) 1190 °C/24 h.

boundaries. Carbon, S and B were detected in the two heat-treated conditions at 1120 °C/4 h and 1190 °C/4 h, as shown in Fig. 3. Si was found only at 1190 °C/4 h, whereas no P was detected in any of the conditions.

3.2. Hot ductility

NST values were 1225 °C for heat treatment conditions of 1120 °C/4 h and 1190 °C/4 h and 1260 °C for 1120 °C/24 h, as listed in Table 3. The peak temperature selected for the on-cooling tests was 1220 °C (average NST – 30) for all the conditions. The on-heating and on-cooling data are plotted in Fig. 4, and the weldability property temperatures are summarised in Table 3.

3.2.1. On-heating

The ductility was relatively low, with no conditions exceeding 25% area reduction. While the ductility measurements after heat treatments at 1120 °C/4 h and 1190 °C/4 h were comparable within the scatter range, the corresponding NDT values were measured at 1140 and 1120 °C, respectively. After being subjected to the homogenisation heat treatments with 24 h exposure time, the NDT was reached at 1140 °C, but with a more severe ductility reduction for 1190 °C/24 h. Interestingly, no evident melting was seen below the NDT when looking at cross-sections and fracture surfaces. Some test samples were subsequently thermally cycled in the Gleeble above the NDT without pulling to fracture or applying a longer holding time to enhance melting. However, the microstructure still appeared unreacted, as visible for the 1120 °C/4 h condition in Fig. 5.

Similarly, no melting was observed below the NDT in the two homogenisation samples at 1190 °C/4 h (Fig. 6 a) and 1190 °C/24 h (Fig. 7). When the test temperature was increased above the NDT, melting was seen to occur in the 1190 °C/4 h condition as a result of the constitutional liquation of MC carbides (Fig. 6 b and c), but the 1190 °C/24 h sample fractured intergranularly without visible melting (Fig. 7 b).

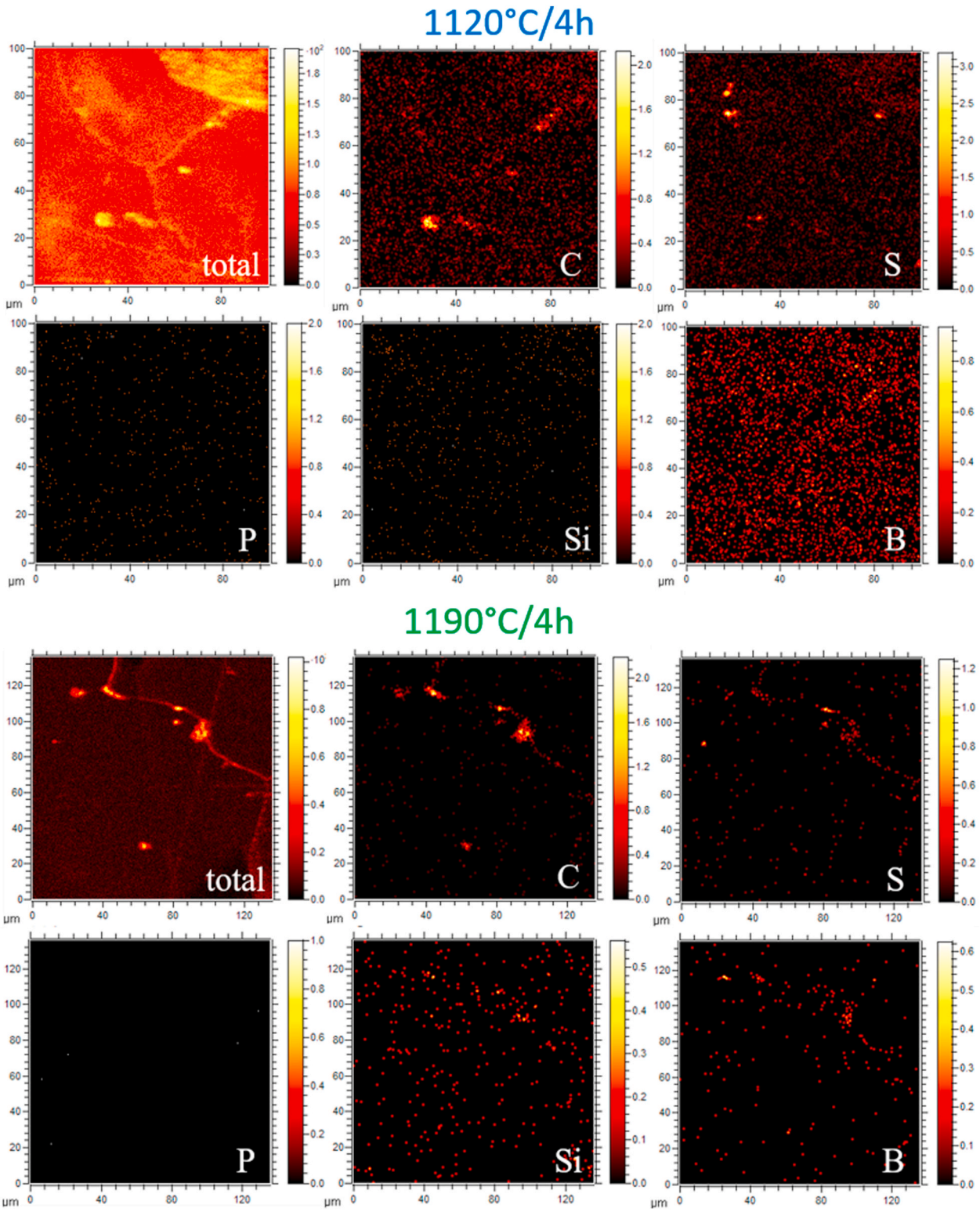

Fig. 3. SIMS elemental map showing the segregation of minor elements in the heat treatments at 1120 °C/4 h and 1190 °C/4 h.

It is interesting to note that the ductility drop to the NDT occurred at 1120 and 1140 °C, which are temperatures below the expected effective solidus of 1160 °C [12].

3.2.2. *On-cooling*

During on-cooling tests, only the heat treatment at 1190 °C/4 h was able to recover to 5% ductility with a corresponding BTR of 120 °C, whereas all other conditions failed to recover ductility during cooling. The inability to undergo ductility recovery was due to extensive melting of the Laves phase and MC carbides in the interdendritic areas for 1120 °C/4 h (Fig. 8 a), whereas constitutional liquation of MC carbides and extensive grain boundary melting had occurred in the long dwell heat treatment at 1120 °C of 24 h (Fig. 8 b). The heat treatment at 1190 °C/4 h that exhibited ductility recovery showed comparatively

Table 3
Summary of different Gleeble testing parameters. All temperatures are in °C, and times are in h.

Temperature	Time	NST	NDT	DRT	BTR
1120	4	1225	1140	–	–
	24	1260	1140	–	–
1190	4	1225	1120	1100	120
	24	NA	1140	–	–

limited melting, mainly from the constitutional liquation of MC carbides and partial grain boundary melting, as visible in Fig. 8 c. In the long dwell heat treatment condition of 1190 °C/24 h, the MC carbides were unreacted. However, grain boundary melting occurred to a greater extent as compared with 1190 °C/4 h (Fig. 8 d)).

Another perspective is obtained by comparing the on-cooling temperature with the NST temperatures of 1225 °C (for the homogenisation heat treatments at 1120 °C/4 h and 1190 °C/4 h) and 1260 °C (for the heat treatment at 1120 °C/24 h). It is interesting to see that in the condition with a lower NDT and with constitutional liquation start temperature of 1140 °C was able to recover the ductility after it was heated to the NST (as the peak temperature and NST coincided), where significant liquid is expected to wet the grain boundaries. On the other hand, the 1120 °C/24 h heat treatment exhibited an NST of 1260 °C, 40 °C higher than the on-cooling peak temperature but was still unable to recover the ductility.

4. Discussion

4.1. Influence of minor elements

The drop in ductility for cast 718Plus started at a very low temperature, suggesting that liquation onset was above 950 °C. Laves phase melting and constitutional liquation of MC carbides did not occur within the temperature range of the ductility drop. This suggests that liquation from grain boundary segregation led to grain boundary embrittlement, as the presence of minor elements is known to lower the solidus temperature [4,5]. However, partial melting along grain boundaries was not observable in SEM. Segregation of Si, C, B and S was detected at grain boundaries of homogenised heat treatment in SIMS analysis. Fig. 9 shows an elemental mapping along a liquated grain boundary after the on-cooling test. The segregation of Si and C is in agreement with what is reported in the previous study on cast Alloy 718 [13]. The role of Si in the weldability of 718Plus has not been previously investigated. Si may be a byproduct of the dissolution of the Laves phase, which was also seen to occur in cast Alloy 718. Si was seen to lower the solubility of Nb in Ni, thereby shifting the solidus temperature to lower values and allowing more Nb to segregate [14,15]. Additions of C in Nb-bearing alloys have been reported to be beneficial to solidification cracking resistance [16]. When present at the grain boundaries in the HAZ, C may be beneficial, as it has been reported to prevent or lower the segregation extent of P and B [17,18], therefore reducing the detrimental effect of these elements on the liquation cracking susceptibility. The presence of C and B is likely to be related to the non-equilibrium segregation mechanism that occurs during fast cooling from heat treatment at a high homogenisation

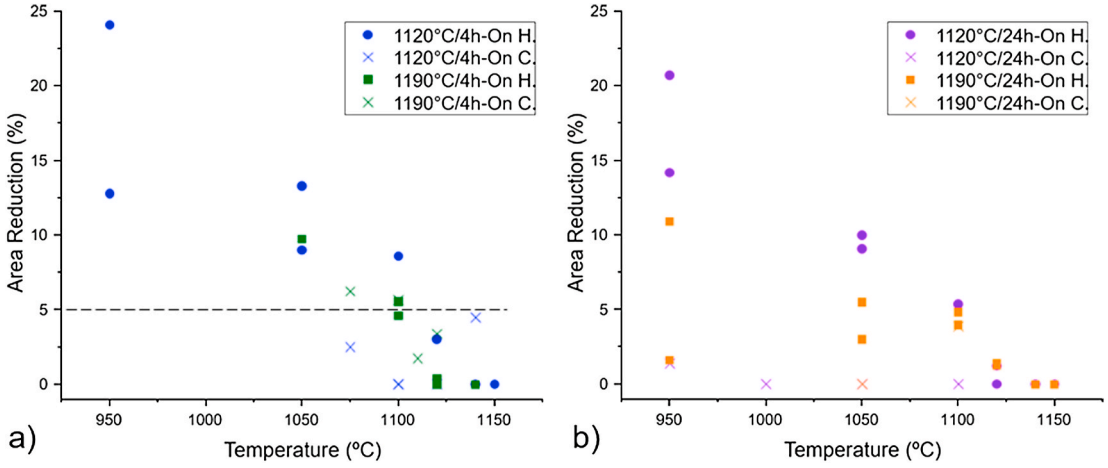

Fig. 4. On-heating (On H.) and on-cooling (On C.) curves at (a) 4 h and (b) 24 h.

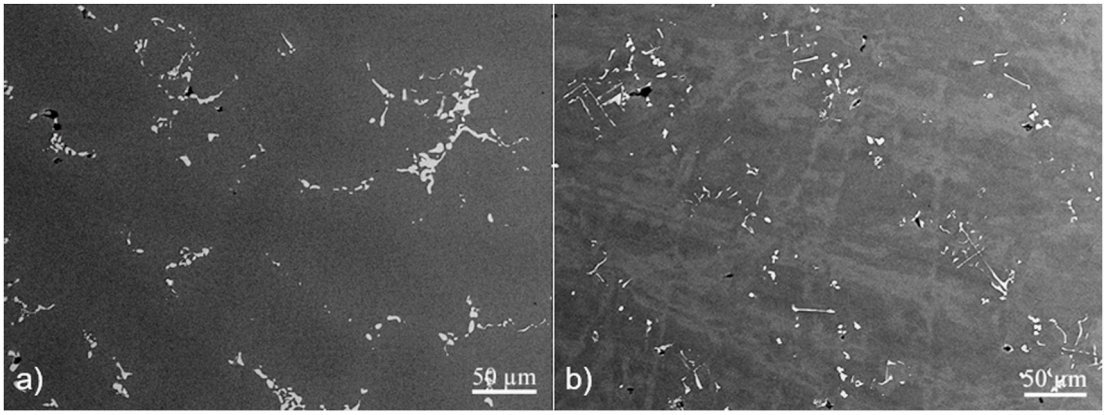

Fig. 5. SEM-BS images showing (a) 1120 °C/4 h and (b) 1120 °C/24 h Gleeble cycled at 1150 °C for 1 s showing the unreacted microstructure.

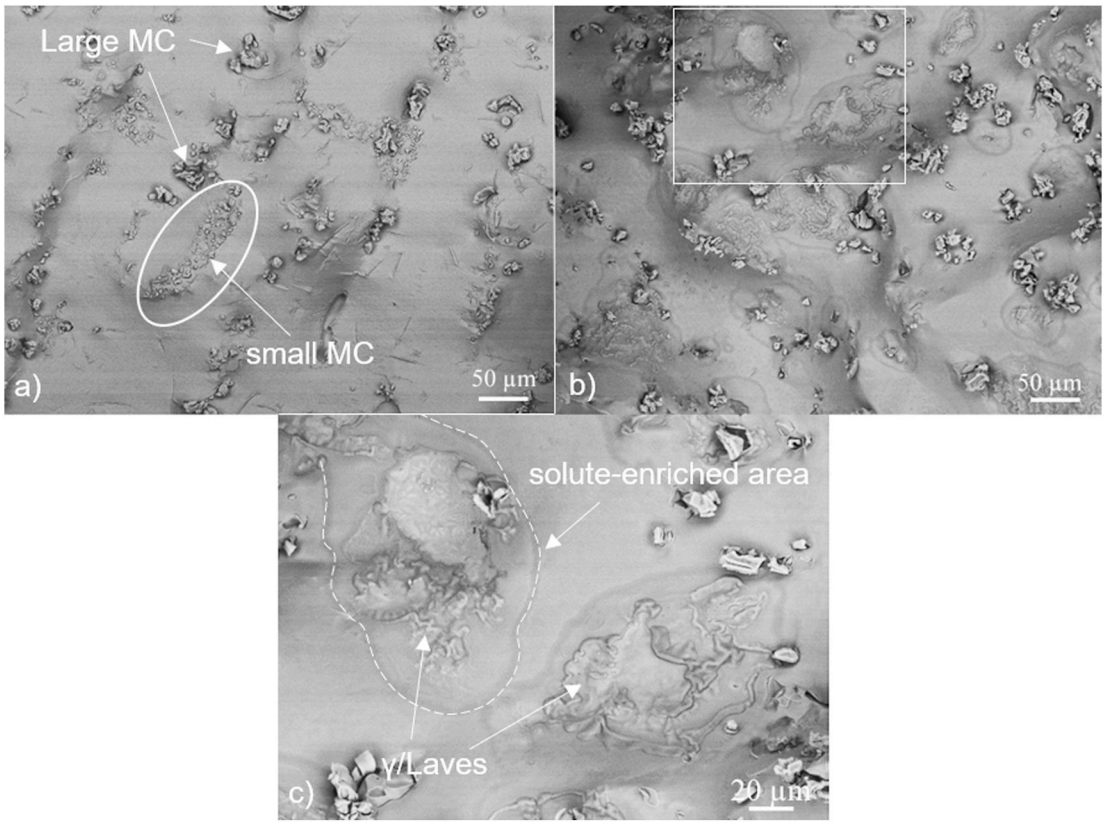

Fig. 6. SEM - SE fracture surface images of on-heating samples of 1190 °C/4 h tested at (a) 1120 °C, showing unreacted carbides, (b) and (c) at 1140 °C, showing constitutional liquation of MC carbides.

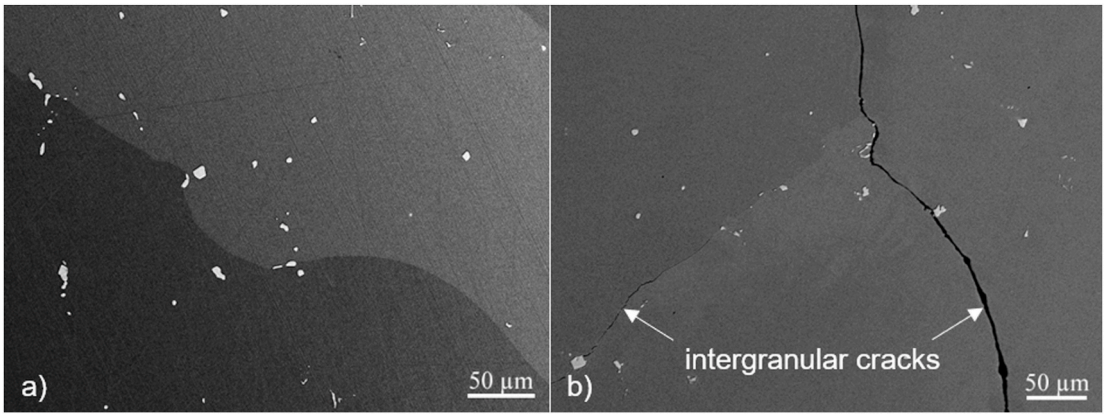

Fig. 7. SEM-BS images showing (a) unaffected microstructure of 1190 °C/24 h Gleeble-cycled at 1140 °C for 1 s without pulling, (b) unaffected microstructure of 1190 °C/24 h cycled at 1150 °C for 0.03 s with intergranular cracks without pulling.

temperature [19,20]. The presence of B is seen to be effective in lowering the liquation temperature as well as extending the BTR on-cooling, which is in agreement with previous studies [4,5]. It should be noted that the SIMS analysis for B detection was conducted only on samples homogenised with 4 h dwell times and not those with 24 h dwell times. This is because the non-equilibrium segregation is largely dependent on the starting heat treatment temperature and the cooling rate from the heat treatment rather than dwell time [19]. Therefore, a greater extent of non-equilibrium segregation was expected in the homogenised conditions with short and long dwell heat treatments at 1190 °C. Furthermore, S, which, according to the authors' knowledge, has not been reported to segregate in wrought or cast 718Plus, is another element that can suppress the solidus temperature. Therefore, it is suggested that the interplay of Si, C, B and S contributes to solute segregation, which causes grain boundary embrittlement below the expected equilibrium solidus of the alloy.

4.2. Influence of Nb

The role of Nb was also investigated by JMatPro simulations and diffusion calculations. As seen from the SEM images (cf. Fig. 2), homogenisation heat treatments were able to dissolve the Nb-rich Laves phase to different extents, with homogenisation efficacy increasing with temperature and dwell time. With the partial dissolution of the Nb-rich Laves phase in the homogenisation heat treatment at 1120 °C/4 h, the Laves phase contributed to liquation. In other homogenisation

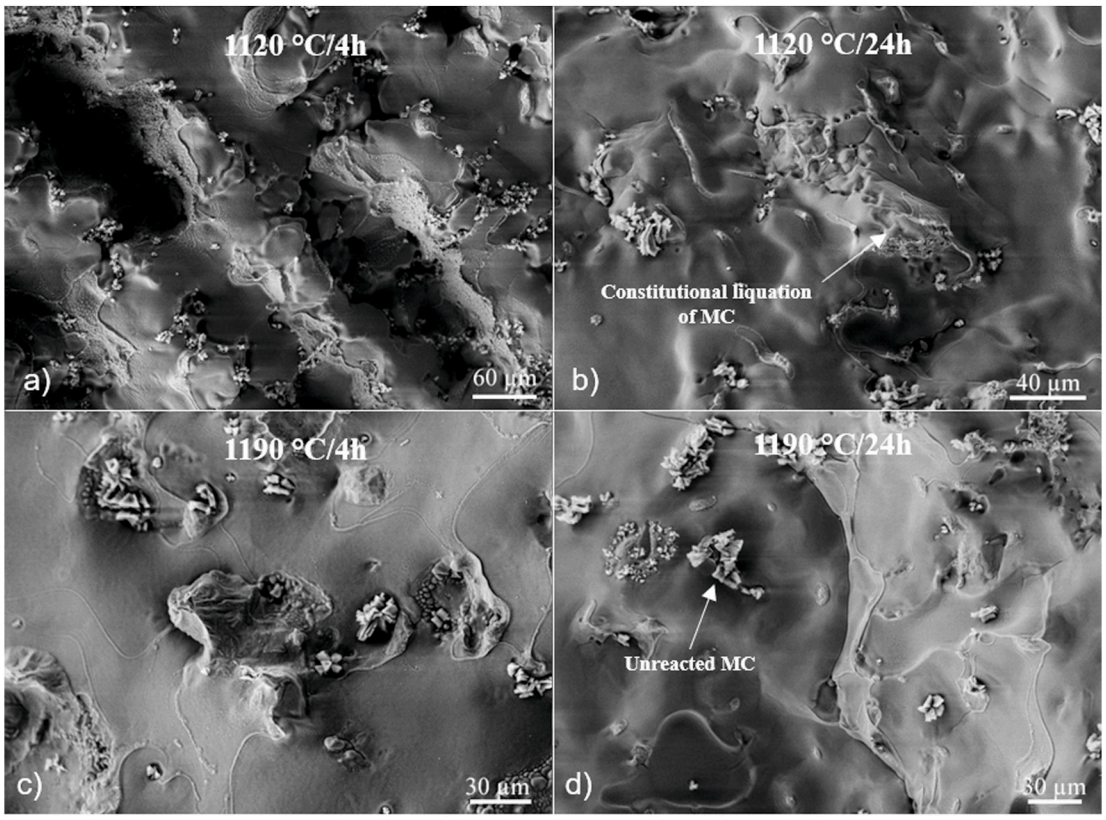

Fig. 8. SEM images taken after on-cooling tests, showing (a) liquation along interdendritic areas in 1120 °C/4 h pulled at 1120 °C and (b) 1120 °C/24 h pulled at 1100 °C; (c) constitutional liquation of carbides at the grain boundary in 1190 °C/4 h pulled at 1120 °C and (d) grain boundary melting in 1190 °C/24 h pulled at 1100 °C.

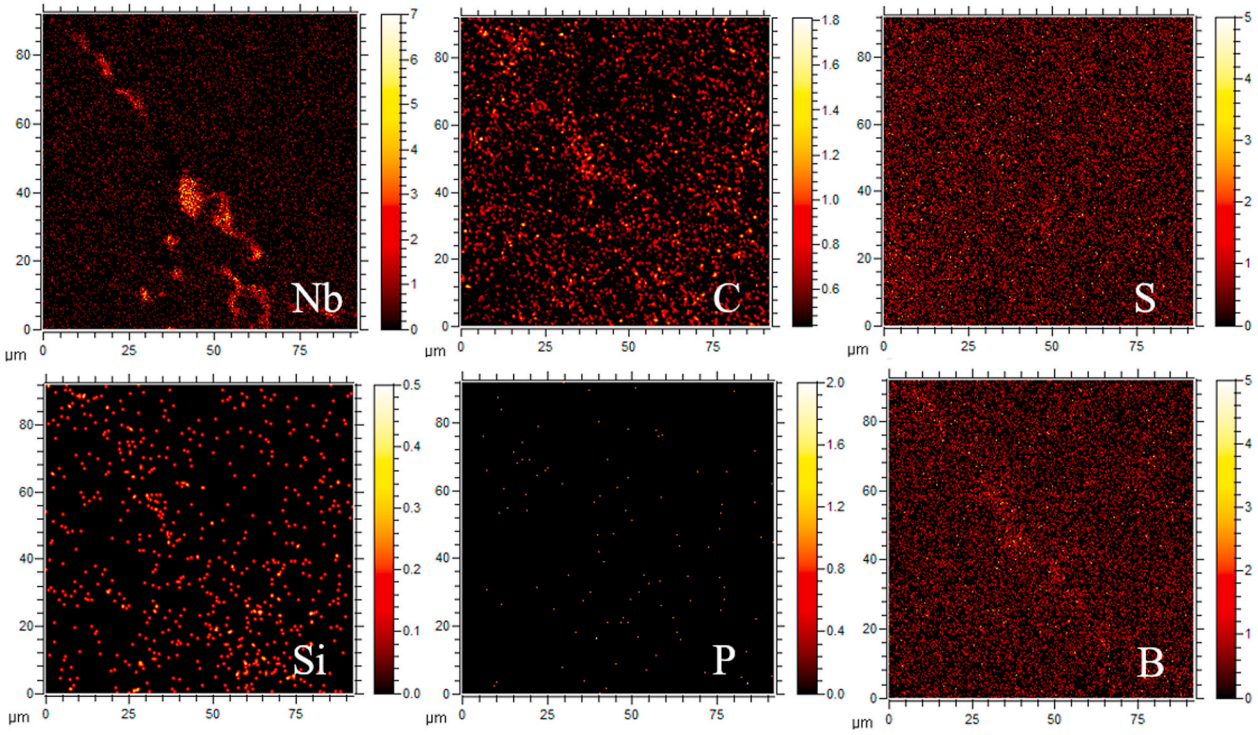

Fig. 9. SIMS elemental map showing the segregation of Nb, C, Si and B at a liquated grain boundary after the on-cooling test in the homogenisation heat treatment at 1190 °C/4 h.

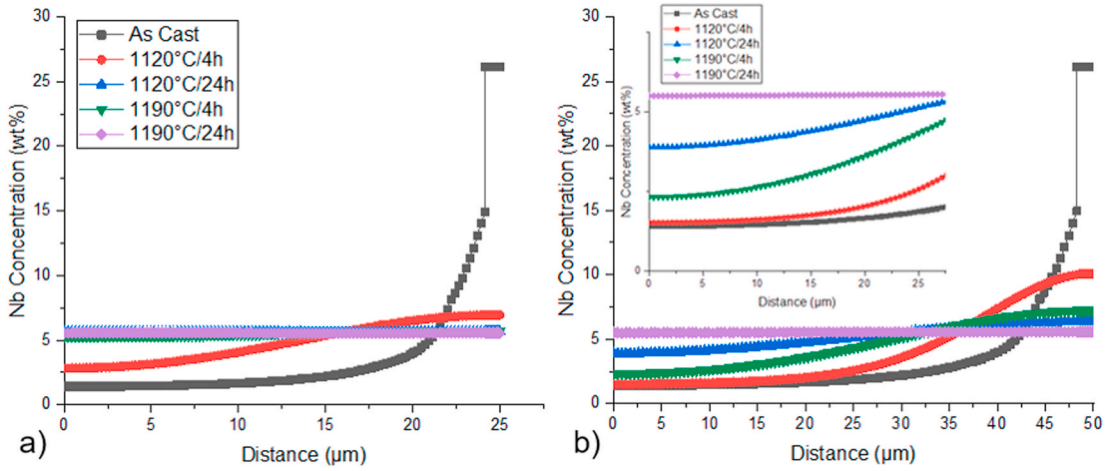

Fig. 10. JMatPro simulations showing homogenisation of Nb in dendrite cores with SDAS of (a) 50 μm and (b) 100 μm.

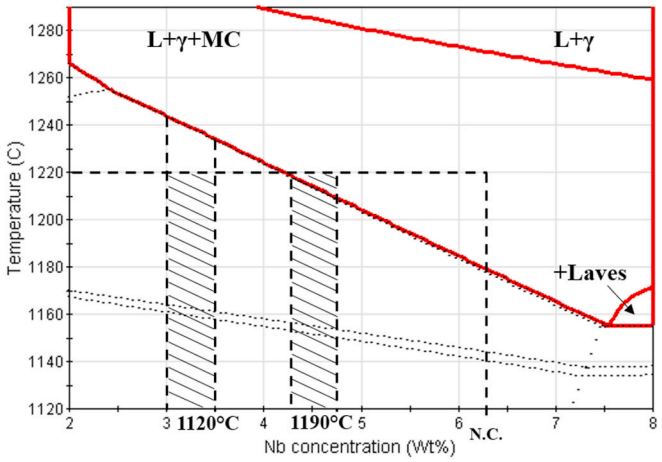

Fig. 11. JMatPro isopleth diagram showing solidus temperature change with variation in Nb concentration, Ni balance. Nominal composition (N.C.) and compositions corresponding to the heat treatments are highlighted with dashed lines corresponding to the intersection with on-cooling peak temperature.

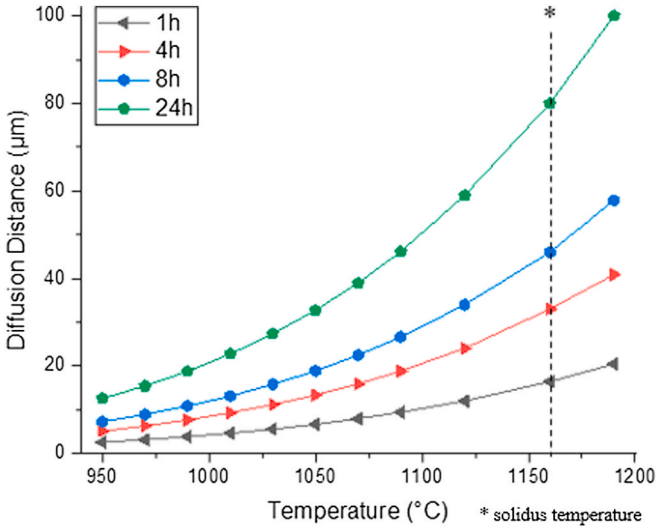

Fig. 12. Calculated diffusion distances for Nb at various homogenisation heat treatment temperatures and times.

treatments, with the dissolution of the Laves phase in the interdendritic areas and subsequent diffusion of Nb, the Nb content was increased in the dendrite cores, as shown in Fig. 10. Considering two scenarios with secondary dendrite arm spacing (SDAS) of 50 and 100 μm, homogenisation would be able to reach the Nb level close to the nominal level in the case of heat treatment at 1190 °C/4 h and similarly for the two long dwell heat treatments at 24 h at SDAS of 50 μm (Fig. 10 a). Since the SDAS was about 100 μm, the homogenisation effect was enhanced in long dwell heat treatments at 24 h, as the Nb atoms were able to diffuse over longer distances.

The isopleth diagram in Fig. 11 shows how different amounts of Nb in the matrix affect the solidus temperature. EDS measurements from the matrix cores between 3 and 3.5 wt % Nb at 1120 °C/4 h and between 4.3 and 4.7 wt % at 1190 °C/4 h are highlighted in Fig. 11. It can be seen that with core compositions present at 1120 °C/4 h, the on-cooling peak temperature is well below the solidus, whereas at 1190 °C/4 h, it crosses the solidus line. Even though the phase diagram is valid under equilibrium conditions, comparably more melting would be expected in the latter case. In the case of long dwell homogenisation heat treatments with more Nb released to the matrix, as suggested by Fig. 10, the composition would shift towards the right side to the highlighted values, thereby suggesting more extensive melting. This is in agreement with the fracture surface images in Fig. 8, where more extensive grain boundary liquation with an enhanced homogenisation level is evident.

Another effect from Nb was through the remelting of MC carbides, which was seen to occur during heat treatment at 1190 °C/4 h. From Fig. 11, it can be seen that the heat treatment temperature is in the lower range of the solidus. It is also possible that the carbides liquated via a constitutional liquation mechanism at this temperature. In order to propose an explanation, diffusion calculations were used. The magnitude of diffusion of Nb in Ni was determined by

$$D = D_0 \times exp(Q/RT) \quad (1)$$

where D_0 is the material constant for Nb of 8.8×10^{-5} m^2/s, Q is −257 kJ/mol, R is 8.31451 J/molK, T is the absolute temperature in K and D is the diffusion coefficient of Nb in a Ni matrix (in m^2/s) [21]. Knowing the diffusion coefficients at various temperatures and times t (in s), diffusion distance l can be obtained by

$$l = \sqrt{2Dt} \quad (2)$$

Diffusion distances at various heat treatment temperatures and dwell times are plotted in Fig. 12. The diffusion distances at a temperature of 1190 °C for the 4 h and 24 h dwell times were 40 and 100 μm, respectively.

Diffusion is supposed to be high enough at 1190 °C/4 h to partially

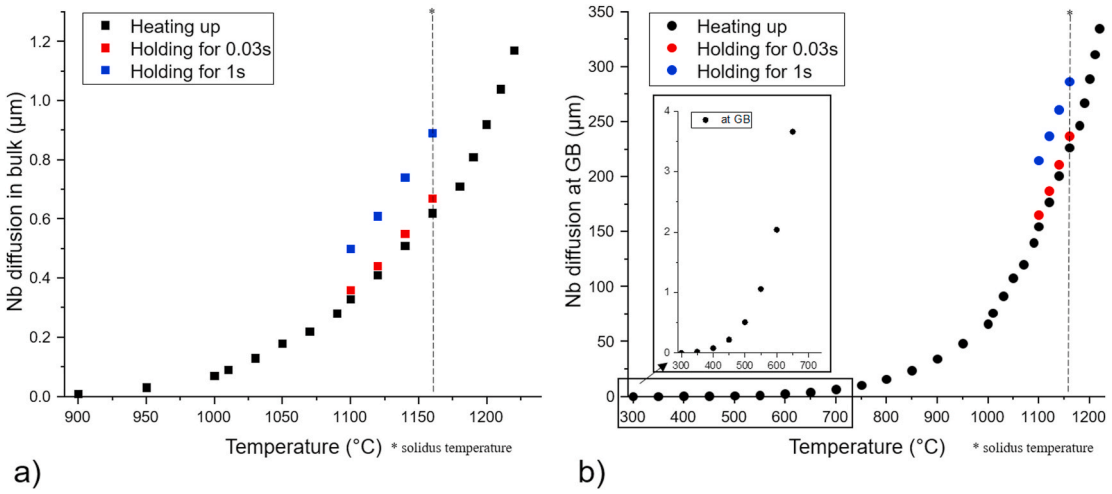

Fig. 13. Diffusion distances during the heating cycle at Gleeble and at different holding times (a) in the matrix and (b) at grain boundaries. Note the difference in the y-axis scale.

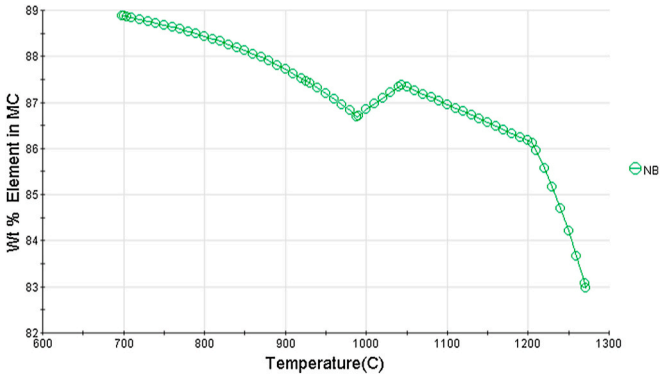

Fig. 14. JMatPro simulation showing the composition stability of MC carbide as a function of temperature.

dissolve the carbides, so the Nb would pile up in the proximity of the carbides and cause melting. However, once the eutectic structure has formed, the heat treatment should be able to dissolve the eutectic if given enough time for diffusion. This would suggest that the carbide liquation happened towards the end of the heat treatment. Assuming that constitutional liquation had also occurred for 1190 °C/24 h during the HIP treatment, the long dwell time would have provided enough time for the dissolution of the liquated structure.

Similarly, in order to verify if constitutional liquation of carbides is possible during the heating cycle in Gleeble tests, the diffusion distances of Nb were calculated in the bulk and at the grain boundaries. At grain boundaries, the extent of diffusion is greater because of the lower activation energy required. Diffusion distances were estimated assuming the same D_0 in the bulk, as no self-diffusion coefficients for Nb were found in the literature, and assuming that the activation energy (Q) at the grain boundary is half of that of the bulk, which is a good approximation in fcc metals [22]. Diffusion coefficients were recalculated using Eq. (1); distances were calculated using Eq. (2) and are plotted in Fig. 13.

According to the calculations, diffusion at grain boundaries started at around 400 °C, well below the temperature in the matrix, which is expected to be around 950 °C. At 1140 °C, the temperature at which constitutional liquation occurred, diffusion distances were about 0.5 and 200 μm, respectively. The magnitude of diffusion at the grain boundary shows that constitutional liquation is possible at these temperatures.

Fig. 14 shows that MC carbides were rather stable up to 1200 °C, after which they dissolved into the matrix when they were exposed to isothermal heat treatments. Appreciable dissolution and diffusion account for only one of the requirements for the constitutional liquation of carbides. Weiss et al. [23] have identified constitutional liquation to be interactions between the heating rate, kinetics of the dissolution of precipitates, minimum solidus temperature and homogenisation of the

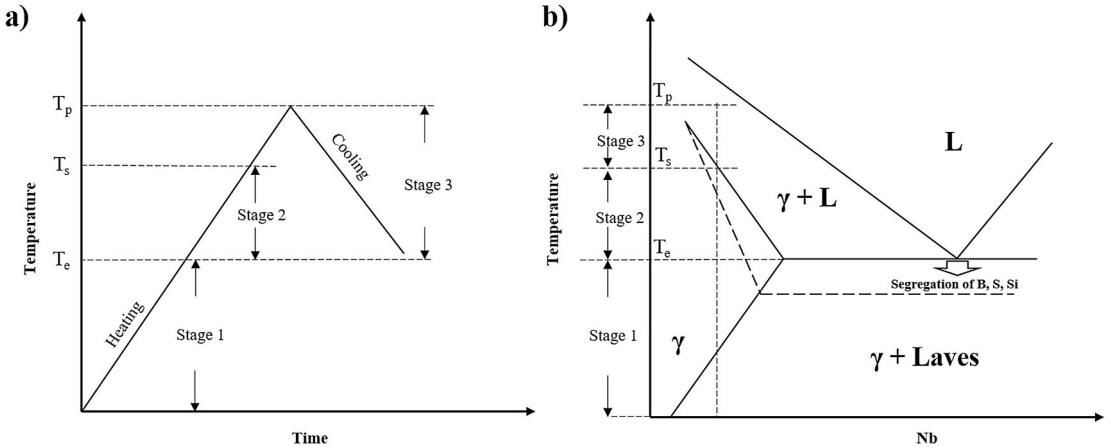

Fig. 15. (a) HAZ cycle divided into three stages based on the temperatures and (b) corresponding pseudo-binary phase diagram for cast 718Plus. Adapted from Ref. [24].

elements from the precipitate into the matrix. As for the previous diffusion considerations, the kinetics of precipitate dissolution were assumed to be governed by the long-term diffusion of Nb, therefore neglecting the shape factor of the precipitates. This suggests that the different minimum solidus temperatures were an important factor in the constitutional liquation of carbide in the current study. As found from the SIMS analysis, the segregation of minor elements lowered the solidus temperature, with a major effect of segregation after homogenisation heat treatment at 1190 °C/4 h. The constitutional liquation along the grain boundaries during the on-heating test could be related to the more severe segregation of minor elements. However, this does not explain the intragranular constitutional liquation during the homogenisation heat treatment, as the minor elements do not segregate in the matrix. Moreover, as mentioned above, the extent of non-equilibrium segregation should be similar in the two homogenisation heat treatments at 1190 °C. This suggests that the minimum solidus temperature and the local composition around the carbides are important factors in the liquation mechanism. The previous considerations do not take into account the diffusion gradient between the carbide and the matrix. With lower Nb in the matrix in the 1190 °C/4 h treatment, especially for large SDAS (Fig. 10), the concentration gradient would be higher, assuming that the composition of MC carbides does not vary significantly after the homogenisation heat treatments, which consequently would accelerate the diffusion. In contrast, in the homogenisation heat treatment at 1190 °C/24 h, the concentration gradient would be lower, as Nb would be able to diffuse for longer distances, reducing the diffusion rate and consequently the release of Nb from carbides into the matrix. Therefore, the dissolution of the MC carbides would be slower.

4.3. Liquation mechanism in cast 718Plus

The liquation mechanism in cast 718Plus during thermal cycling is a combination of different contributing factors, as discussed in the previous sections. The liquation mechanism is summarised in Fig. 15.

The HAZ cycle is divided into three stages based on temperature ranges between the eutectic temperature (T_e), solidus temperature (T_s) and peak temperature (T_p), which are highlighted in the pseudo-binary phase diagram. Stage 1 (up to T_e) is characterised by the dissolution of Nb-rich phases, with a higher diffusion rate along the grain boundaries as compared with the grain interior. In this stage, liquation occurs from the solute segregation of minor elements, which lowers the effective solidus of the alloy. In Stage 2 (between T_e and T_s), liquation is possible from the melting of the Laves phase or by constitutional liquation of MC carbides, depending on the chemistry resulting after the homogenisation heat treatments. In Stage 3 (between T_s and T_p), bulk melting occurs, with the extent of melting based on the amount of Nb in solid solution. The overall contribution will depend on the contribution from solute segregation, Laves melting, constitutional liquation of MC carbides and supersolidus melting of the matrix. From the considerations regarding the liquation characteristics and the hot ductility results, it can be said that the extent of liquation determines the hot ductility of the material. This is supported by the observation that the homogenisation heat treatment at 1190 °C/4 h with the least extent of liquation was able to recover its ductility during on-cooling tests. It is likely that the contribution from solute segregation is similar when it comes to C, Si and S. The effect from the non-equilibrium segregation of B is, however, likely to be more severe in the higher homogenisation heat treatment temperatures at 1190 °C. The contribution to liquation from the constitutional liquation of MC carbides can be assumed to be rather limited, as their area fraction was estimated to only 0.5 wt % [7]. At the same time, the homogenisation heat treatment at 1190 °C/24 h, which would have similar solute segregation of minor alloying elements to that of the former, exhibited zero ductility on-cooling. This suggests that the effect of Nb on lowering the solidus temperature and therefore on enhancing bulk melting was more pronounced in the long dwell homogenisation heat treatments.

5. Conclusions

The hot ductility of cast 718Plus was investigated, and the liquation behaviour of the material was correlated to the microstructural evolution after homogenisation heat treatments. The following conclusions can be drawn from the results:

- Heat treatments at 1120 °C/4 h and 1190 °C/4 h exhibited similar on-heating ductility. The latter had the lowest NDT at 1120 °C, with the constitutional liquation of MC carbides starting at 1140 °C. This was also the only condition to recover its ductility on-cooling at 1100 °C, resulting in a BTR of 120 °C.
- The long-dwell heat treatment at 1190 °C/24 h exhibited the lowest overall ductility. Both homogenisation heat treatments at 1120 °C/24 h and 1190 °C/24 h reached the NDT at 1140 °C.
- The segregation of minor elements such as S and B contributed to liquation below the expected solidus of the material. The effective role of Si and C needs to be further investigated.
- Liquation was mainly caused by the melting of the partially dissolved Laves in material heat-treated at 1120 °C/4 h. The heat treatment at 1190 °C/4 h exhibited extensive constitutional liquation and partial grain boundary melting. The main contribution to liquation in the 24 h dwell time heat treatments was the extensive supersolidus melting of grain boundaries due to enhanced homogenisation of Nb, which lowered the solidus. In the heat treatment at 1120 °C/4 h, constitutional liquation of MC carbides also occurred.
- The hot ductility results are in agreement with previously published Varestraint test results that showed a higher HAZ liquation cracking susceptibility of the heat-treated alloy at 1120 °C/24 h and 1190 °C/24 h than that at 1120 °C/4 h and 1190 °C/4 h. The higher cracking susceptibility of the 24 h long heat treatments can be attributed to the more extensive grain boundary liquation.

CRediT authorship contribution statement

Sukhdeep Singh: Conceptualization, Data curation, Investigation, Methodology, Writing - original draft. **Fabian Hanning:** Investigation, Writing - review & editing. **Joel Andersson:** Funding acquisition, Supervision, Writing - review & editing.

Declaration of competing interest

The authors declare that they have no known competing financial interests or personal relationships that could have appeared to influence the work reported in this paper.

Acknowledgements

Per Malmberg at the Department of Chemistry at Chalmers University of Technology is acknowledged for the SIMS analysis. The authors highly appreciate the financial support from SpaceLAB through European Regional Development Fund and GKN Aerospace Sweden AB.

References

[1] W.D. Cao, R. Kennedy, Role of chemistry in 718-type alloys–Allvac® 718Plus™ alloy development, Superalloys (2004) 91–99, 2004.
[2] W.D. Cao, Solidification and solid state phase transformation of Allvac® 718Plus™ alloy. Superalloys 718, 625 and Various Derivatives 2005, 2005, pp. 166–177.
[3] B. Peterson, et al., Castability of 718Plus (®) alloy for structural gas turbine engine components. 7th International Symposium on Superalloy 718 and Derivatives, 2014, pp. 131–146.
[4] K.R. Vishwakarma, M.C. Chaturvedi, A study of HAZ microfissuring in a newly developed allvac 718 Plus superalloy, Superalloy (2008) 241–250, 2008.
[5] K.R. Vishwakarma, M.C. Chaturvedi, Effect of boron and phosphorus on HAZ microfissuring of Allvac 718 Plus superalloy, Mater. Sci. Technol. 25 (3) (2009) 351–360.
[6] S. Singh, J. Andersson, Varestraint weldability testing of cast ATI® 718Plus™—a comparison to cast Alloy 718, Weld. World 63 (2) (2019) 389–399.

[7] F. Hanning, A.K. Khan, J. Andersson, O. Ojo, Advanced Microstructural Characterisation of Cast ATI 718Plus®—Effect of Homogenisation Heat Treatments on Secondary Phases and Repair Welding Behaviour, Weld. World, 2020.
[8] M.L. Barron, Crack Growth-Based Predictive Methodology for the Maintenance of the Structural Integrity of Repaired and Nonrepaired Aging Engine Stationary Components, GE AIRCRAFT ENGINES CINCINNATI OH, 1999.
[9] S.M. Snyder and E.E. Brown, Laves free cast + hip nickel base superalloy. U.S. Patent No 4,750,944, 1988.
[10] D.F. Paulonis, J.J. Schirra, Alloy 718 at Pratt & Whitney–Historical Perspective and Future Challenges, Superalloys, 2001, pp. 13–23.
[11] S. Singh, J. Andersson, Heat-Affected-Zone Liquation Cracking in Welded Cast Haynes® 282®, Metals, 2020, p. 11.
[12] S. Singh, Varestraint Weldability Testing of Cast Superalloys, Licentiate Thesis, Chalmers University of Technology, 2018.
[13] S. Singh, F. Hanning, J. Andersson, Influence of hot isostatic pressing on hot ductility of cast Alloy 718: the effect of Niobium and minor elements on liquation mechanism, Metall. Mater. Trans. A, 2020. In press.
[14] Y. Zhu, et al., Effect of P, S, B and Si on the solidification segregation of inconel 718 alloy, Superalloys 718 625 (706) (1994) 89–98. Various Derivatives, 1994.
[15] J.T. Guo, L.Z. Zhou, The effect of phosphorus, sulphur and silicon on segregation, solidification and mechanical properties of cast Alloy 718, Superalloys, 1996, pp. 451–455.
[16] J.N. Dupont, A.R. Marder, C.V. Robino, Solidification and weldability of Nb-bearing superalloys, Weld. J. 77 (10) (1998) 417s–431s.
[17] T. Alam, P.J. Felfer, M.C. Chaturvedi, L.T. Stephenson, M.R. Kilburn, J.M. Cairney, Segregation of B, P, and C in the Ni-based superalloy, inconel 718, Metall. Mater. Trans. 43 (7) (2012) 2183–2191.
[18] S. Benhaddad, N.L. Richards, U. Prasad, H. Guo, M.C. Chaturvedi, The influence of B, P and C on heat-affected zone micro-fissuring in inconel type superalloy. Superalloys 2000 (Ninth International Symposium), 2000, pp. 703–711.
[19] L. Karlsson, H. Nordén, H. Odelius, Overview no. 63 Non-equilibrium grain boundary segregation of boron in austenitic stainless steel—I. Large scale segregation behaviour, Acta Metall. 36 (1) (1988) 1–12.
[20] L. Karlsson, H. Nordén, Overview no. 63 Non-equilibrium grain boundary segregation of boron in austenitic stainless steel—IV. Precipitation behaviour and distribution of elements at grain boundaries, Acta Metall. 36 (1) (1988) 35–48.
[21] M.S.A. Karunaratne, R.C. Reed, Interdiffusion of niobium and molybdenum in nickel between 900-1300 C, in: Defect and Diffusion Forum, vol. 237, Trans Tech Publications Ltd, 2005, pp. 420–425.
[22] D.A. Porter, K.E. Easterling, M.Y. Sherif, Phase Transformations in Metals and Alloys, (Revised Reprint), CRC Press, 2009.
[23] B. Weiss, G.E. Grotke, R. Stickler, Physical metallurgy of hot ductility testing, Weld. J. 49 (10) (1970) 471s.
[24] B. Radhakrishnan, R.G. Thompson, A model for the formation and solidification of grain boundary liquid in the heat-affected zone (HAZ) of welds, Metall. *Trans. A* 23 (6) (1992) 1783–1799.